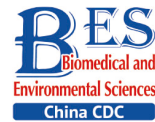**Original Article**

Global Profiles of Acetylated Proteins in Brains of Scrapie Agents 139A- and ME7-Infected Mice Collected at Mid-Early, Mid-Late, and Terminal Stages[*]

SHI Qi[1,2,3,&], CHEN Dong Dong[1,2,&], ADALATI Maimaitiming[1,2], XIAO Kang[1,2], GAO Li Ping[1,2],

YANG Xue Hua[1,2], WU Yue Zhang[1,2], CHEN Cao[1,2,4], and DONG Xiao Ping[1,2,3,4,5,#]

1. State Key Laboratory of Infectious Disease Prevention and Control, NHC Key Laboratory of Medical Virology and Viral Diseases, National Institute for Viral Disease Control and Prevention, Chinese Center for Disease Control and Prevention, Beijing 102200, China; 2. Collaborative Innovation Center for Diagnosis and Treatment of Infectious Diseases, Zhejiang University, Hangzhou 310014, Zhejiang, China; 3. China Academy of Chinese Medical Sciences, Beijing 100000, China; 4. Center for Biosafety Mega-Science, Chinese Academy of Sciences, Wuhan 430000, Hubei, China; 5. Shanghai Institute of Infectious Disease and Biosafety, Shanghai 201318, China

Abstract

Objective   To describe the global profiles of acetylated proteins in the brains of scrapie agents 139A- and ME7-infected mice collected at mid-early, mid-late, and terminal stages.

Methods   The acetylated proteins from the cortex regions of scrapie agent (139A- and ME7)-infected mice collected at mid-early (80 days postinfection, dpi), mid-late (120 dpi), and terminal (180 dpi) stages were extracted, and the global profiles of brain acetylated proteins were assayed with proteomic mass spectrometry. The proteins in the infected mice showing 1.5-fold higher or lower levels than that of age-matched normal controls were considered as differentially expressed acetylated peptides (DEAPs).

Results   A total of 118, 42, and 51 DEAPs were found in the brains of 139A-80, 139A-120, and 139A-180 dpi mice, respectively. Meanwhile, 390, 227, and 75 DEAPs were detected in the brains of ME7-80, ME7-120, and ME7-180 dpi mice, respectively. The overwhelming majority of DEAPs in the mid-early stage were down-regulated, and more portions of DEAPs in the mid-late and late stages were up-regulated. Approximately 22.1% (328/1,485) of acetylated peptides mapped to 74 different proteins were mitochondrial associated. Kyoto Encyclopedia of Genes and Genomes pathway analysis identified 39 (80 dpi), 13 (120 dpi), and 10 (180 dpi) significantly changed pathways in 139A-infected mice. Meanwhile, 55, 25, and 18 significantly changed pathways were observed in the 80, 120, and 180 dpi samples of 139A- and ME7-infected mice ($P < 0.05$), respectively. Six pathways were commonly involved in all tested samples. Moreover, many steps in the citrate cycle (tricarboxylic acid cycle) were affected, represented by down-regulated acetylation for relevant enzymes in the mid-early stage and up-regulated acetylation in the mid-late and late stages.

Conclusion   Our data here illustrated the changes in the global profiles for brain acetylated proteins during prion infection, showing remarkably inhibited acetylation in the early stage and relatively enhanced acetylation in the late stage.

Key words: Prion; Scrapie-infected mouse; Acetylation; Proteomics; Kyoto Encyclopedia of Genes and Genomes pathway

INTRODUCTION

Prion disease is a group of transmissible neurodegenerative disorders affecting a species of animals and humans[1]. The etiological agent is a prion, a unique pathogen without nucleic acid. Besides the neuropathological hallmarks of prion disease, such as prion deposits (PrP^{Sc}), neuron loss, and gliosis, numerous abnormalities of biological pathways in the central nervous system (CNS) have been identified, e.g., increased inflammatory reactions, activated autophagy, and evident apoptosis[2-5], which result from the aberrant alterations of the transcriptions and expressions of a large number of proteins and enzymes in the brain, as verified by the assays of transcriptomics and proteomics[6-9]. Moreover, abnormal changes in post-translational modifications for brain proteins have been repeatedly described in the CNS tissues of various neurodegenerative diseases, involving phosphorylation, *S*-nitrosylation, ubiquitylation, *O*-GlcNAcylation, acetylation, etc.[10-13].

Protein acetylation, which is regulated by acetylase and deacetylase, is a kind of important reversible protein modification in cells after the translation process[14,15]. This kind of post-translational modification participates actively in the regulation of protein functions, chromosome structure, and gene expressions. The developments and advances in mass spectrometry (MS) enable the localization of most acetylation sites in all proteomics at high resolution. Studies have proposed nearly 3,600 acetylation sites in about 1,750 proteins, suggesting that acetylation modification is one of the most abundant chemical modifications in nature[16-18]. Acetylation may affect various physiological processes of proteins, including chromatin remodeling, cell cycle, splicing, nuclear transport, mitochondrial biology, and actin nucleation. In biology, acetylation plays an important role in immunity, circadian rhythm, and memory formation. Protein acetylation is also a favorite target for the design of new drugs for various diseases.

The changes in acetylation for some proteins have also been reported in the brains of prion diseases. Previously, we have described that the levels and activities of Sirt1, a class III histone deacetylase, remarkably decreased in the brains of different scrapie-infected rodent models and in a prion-infected cell line SMB-S15, resulting in increases in the acetylating forms of some Sirt1 target proteins, such as P53, peroxisome proliferator-activated receptor γ coactivator(PGC)-1, and signal transducer and activator of transcription

factor 3[19]. We have also confirmed the declined levels of Sirt3 in the brain tissues of several scrapie-infected mice and SMB-S15 cells, leading to increases in acetylating forms of superoxide dismutase (SOD) 2 and ATP5β, which subsequently induced the increase in intracellular reactive oxygen species and reduction of ATP, respectively[20]. Aberrant alterations in acetylation modifications for other proteins have also been found in the brain tissues or *in vitro* models of several neurodegenerative diseases, e.g., tau, microtubules and SOD1[21-23]. However, the global change in protein acetylation in the brain tissues of prion diseases remains unsettled. In this study, we systematically analyzed the changes in global profiles of brain acetylated proteins during prion infection based on two scrapie agent-infected mouse models.

MATERIALS AND METHODS

Ethics Approval

All procedures involving live animals were approved by the Ethics Committee of the National Institute for Viral Disease Control and Prevention. All protocols were designed to minimize animal discomfort. The approval identifications for this study are found in animal use document 2013031.

Brain Samples of Scrapie-infected Experimental Mice

The brain samples of cortex regions from scrapie agent (139A- and ME7)-infected mice collected at 80, 120, and 180 dpi were enrolled in this study. Each group consisted of tissues from three individual mice. The animal bioassays and confirmations of the experimental scrapie in the inoculated mice were described previously[24]. The brain samples of three age-matched normal mice from each group were used as the control.

Western Blot

Brain tissues were homogenized in lysis buffer (100 mmol/L NaCl, 10 mmol/L ethylenediaminetetraacetic acid, 0.5% NP-40, 0.5% sodium deoxycholate, 10 mmol/L Tris, and pH 7.4) containing protease inhibitor cocktail set III. The homogenates were centrifuged at 2,000 ×*g* for 10 min, and the supernatant fractions were collected. Aliquots of brain homogenate were separated by 12% sodium dodecyl sulfate-polyacrylamide gel electrophoresis (SDS-PAGE) and electroblotted onto nylon membranes. The membranes were blocked

with Tris-Hcl buffer saline (TBS) containing 5% skimmed milk at room temperature (RT) for 2 h and incubated with various primary antibodies at 4 °C overnight, such as anti-PrP mAb (6D11, sc-58581; Santa Cruz Biotechnology), anti-glial fibrillary acidic protein (GFAP) (#3670; Cell Signaling), anti-Iba1 (sc32725; Santa Cruz Biotechnology), anti-β-actin antibody (1:5,000, Huaxingbio, HX1827). After washing with TBS containing 0.1% Tween 20, the membranes were incubated with horseradish peroxidase-conjugated secondary antibodies (Jackson ImmunoResearch Labs, 115-035-003 and 111-035-003) at RT for 1 h. The blots were developed using an enhanced chemiluminescence system (PerkinElmer, NEL103E001EA) and visualized on autoradiography films (General Electrics). Images were captured by ChemiDoc ™ XRS + Imager and quantified by Image J software.

To detect the presence of proteinase K-resistant PrP^{Sc}, we digested the brain homogenates or cell lysates with a final concentration of 50 μg/mL proteinase K at 37 °C for 1 h prior to Western blots.

Protein Extraction

About 500 mg of brain samples were homogenized by an automatic grinding machine in the lysis buffer (8 mmol/L urea, 30 mmol/L HEPES, 1 mmol/L Na_3VO_4, 2.5 mmol/L NA_3PO_4, and 5 mmol/L $C_4H_7NaO_2$). The lysates were mixed with 10% tricarboxylic acid (TCA)—acetone and precipitated at −20 °C overnight. The precipitates were collected by centrifugation at 20,000 rpm for 30 min and washed thrice with acetone. After the addition of the lysis buffer, the preparations were exposed to ultrasonic (pulse on: 2 s, pulse off: 3 s, and power: 180 W) for 5 min. After centrifugation at 20,000 rpm for 30 min, the supernatants were collected and incubated with 10 mmol/L dithiothreitol final concentration at 56 °C for 1 h. The products were immediately mixed with 55 mmol/L IAM final concentration and stored in the dark for 1 h. The protein concentrations in the products were measured with a Bradford protein assay. The quality of the extracted proteins was evaluated by SDS-PAGE, which showed clear bands (Supplementary Figrue S1A available in www.besjournal.com). The protein quantitative standard curve showed an R^2 value of 0.9932, which fulfilled the requirement of the standard operating procedures (SOP) of the experiment.

Protein Digestion and Peptide Purification

Aliquots of 10 mg proteins from each preparation were transferred to a 10 K ultrafilter and centrifuged at 4,000 rpm at 4 °C for 40 min. After discarding the waste liquid, 5 mL 5 mmol/L triethylbenzylammoniumchloride (TEBA) was added to the filters and centrifuged at 4,000 rpm at 4 °C for 40 min. The above procedures were repeated. The protein digestion was performed with 1 μg/μL trypsin at 37 °C for 24 h. The purification of peptides was conducted with a C18 reversed-phase column to remove salts and dried by vacuum. Measurement of the digested peptides showed that the lengths of the majority were less than 30 amino acids (Supplementary Figure S1B).

Enrichment of Acetylated Peptides

The dried samples were solved in IAP buffer containing 50 mmol/L MOPS (pH 7.2), 10 mmol/L Na_3PO_4, and 50 mmol/L NaCl, and pellets were discarded by centrifuged at 10,000 rpm at 4 °C for 5 min. The enrichment of acetylated peptides was conducted with a commercial kit in accordance with the manufacturer's instructions (ICP0388, ImmuneChem Pharmaceuticals). After washing the acetylated antibody-conjugated beads with phosphate-buffered saline, 2% acetic acid, and IAP buffer, the samples were added and incubated overnight rotatably. The beads were collected by low-speed centrifuge and washed with IPA buffer and double-distilled water.

Peptide Labeling and Identification of Mass Spectra

The enriched acetylated peptides were mixed with 41 μL acetonitrile, vortexed for 1 min, and pelleted after a short centrifuge. Different isotopes were added to the tested peptide preparations, maintained at RT for 1 h, mixed with 8 μL hydroxylamine, and maintained for 15 min. The labeled products were further dried by vacuum.

Desalted peptide mixtures were loaded onto an Acclaim PePmap C18-reversed-phase column (75 μm × 2 cm, 3 μm, and 100 Å; Thermo Scientific) and separated with a reversed-phase C18 column (75 μm × 10 cm, 5 μm, and 300 Å; Agela Technologies) mounted on a Dionex ultimate 3,000 nano LC system. The peptides were eluted using a gradient of 5%–80% (v/v) acetonitrile in 0.1% formic acid over 45 min at a flow rate of 300 nL/min combined with a Q-Exactive mass spectrometer (Thermo Fisher Scientific, MA, USA).

The eluates were directly entered to the Q-Exactive mass spectrometer (Thermo Fisher Scientific, Waltham, MA, USA), which was set in positive ion mode and data-dependent manner with

full MS scan in the range of 350–2,000 m/z, full scan resolution at 70,000, MS/MS scan resolution at 35,000, MS/MS scan with a minimum signal threshold of 1×10^5, and isolation width at 2 Da. To evaluate the performance of this MS in the samples, two MS/MS acquisition modes with a higher collision energy dissociation (HCD) were employed. To optimize the MS/MS acquisition efficiency of HCD, we systemically examined normalized collision energy 30 times with a step of 20%.

Statistical Analysis

Quantitative analysis of immunoblot images was carried out using the software Image J, and the gray values of each target blot were evaluated. Quantitative evaluations of fluorescent intensity in immunofluorescence assays were automatically performed with the Columbus software in Operetta. SPSS18.0 (International Business Machines Corporation, The United States) statistical software was used for statistical work. All data analyses were presented as mean ± standard deviation, and statistical analysis was performed using the t test.

RESULTS

Aberrant Alterations of PrPSc, GFAP, and Iba1 in the Brain Samples of 139A- and ME7-infected Mice Collected at Mid-early, Mid-late, and Terminal Stages

The clinical, neuropathological, and pathogenic features of scrapie agents 139A- and ME7-infected C57 mice were thoroughly described previously. The mean incubation times of the mice infected with agents 139A and ME7 were 183.9 ± 23.1 (154–226) and 184.2 ± 11.8 (165–193) days, respectively[24]. To test the changes in the main hallmarks of prion disease in the brain samples of scrapie-infected mice collected at the mid-early, mid-late, and terminal stages, which were employed in further proteomic assays, we evaluated the levels of PrP^{Sc}, GFAP, and Iba1 by individual-specific Western blots. PK-resistant PrP signals (PrP^{res} or PrP^{Sc}) were detected in all brain samples of scrapie-infected mice, showing three bands ranging from 20 kD to 30 kD (Figure 1A). A quantitative assay of the signal intensities showed that the PrP^{Sc} in the samples at the mid-early stage was weak and became considerably stronger at the mid-late and late stages (Figure 1A). The signals of GFAP (Figure 1B) and Iba1 (Figure 1C) in the brain samples of the scrapie-infected mice displayed a time-dependent increase and had more changes

than the brain tissues of normal mice at the same time point (Supplementary Figure S2 available in www.besjournal.com).

Global Acetylated Proteins Profiles of the Brain Samples of 139A- and ME7-infected Mice Collected at the Mid-early, Mid-late, and Terminal Stages

The homogenates of cortex regions of three individual mice infected with scrapie agents 139A and ME7 collected at mid-early, mid-late, and final stages were pooled as the samples of 139A-80, 139A-120, and 139A-180 dpi and ME7-80, ME7-120, and ME7-180 dpi. Meanwhile, the homogenates of cortex regions of three age-matched individual normal mice were pooled as the normal control. The quality of extracted proteins, quantitative accuracy of proteins, trypsin hydrolysis efficiency, mass spectral mass deviation, MS acquisition intensity, and data volume fulfilled the requirements of the quality control for proteomic assays. A total of 271,383 MS/MS spectra were achieved, and 63,365 of them were matched spectra. Meanwhile, 2,250 proteins elicited from 7,831 unique peptides were identified with a 95% confidence interval by the PeptideProphet Algorithm. A total of 1,485 acetylated peptides were identified.

The differentially expressed acetylated peptides (DEAPs) in the brains of scrapie-infected and normal mice were calculated based on the SOP for TMT proteomics in Beijing Institute of Genomics, Chinese Academy of Science, and other published data[6,25]. Out of 1,485 acetylated peptides, the DEAPs (change > 1.5-fold) in the brains of 139A-80, 139A-120, and 139A-180 dpi were 118 (7.9%), 42 (2.8%), and 51 (3.4%), respectively. Meanwhile those in the brains of ME7-80, ME7-120, and ME7-180 dpi were 390 (26.3%), 227 (15.3%), and 75 (5.1%), respectively (Figure 2A). The DEAPs (change > 2.0-fold) in the brains of 139A-80, 139A-120, and 139A-180 dpi were 8 (0.54%), 5 (0.34%) and 6 (0.4%), and those in the brains of ME7-80, ME7-120, and ME7-180 dpi were 91 (6.1%), 36 (2.4%), and 12 (0.81%) respectively (Figure 2B). Notably, considerably more decreased DEAPs were observed in the brain samples of the early stage, and more increased DEAPs were identified in the mid-late and late stages of 139A- and ME7-infected mouse groups with > 1.5- and > 2.0-fold (Figure 2). Additionally, more DEAPs were found in the brains of ME7-infected mice at every time point than those of 139A-infected mice. To explore the potential changes in proteomic profiles among the different brain samples maximally, we used the peptides that were > 1.5-fold increased or

decreased as DEAPs in this study.

Profiles of DEAPs in Mitochondria of the Brain Samples of 139A- and ME7-infected Mice Collected at the Mid-early, Mid-late, and Terminal Stages

Out of 1,485 identified acetylated peptides, 328 peptides were marked as mitochondrial organism (OS), which accounted for 22.1% of total acetylated peptides. A total of 135 acetylated peptides (41.1%) showed differential expression (> 1.5-fold increased and/or < 0.666-fold decreased) in one or more

tested samples of scrapie-infected mice. Figure 3A illustrates the numbers of DEAPs in the samples at each time point of the two scrapie-infected mice. Similar to the global profile of DEAPs, the numbers of DEAPs in the brain samples of mid-early stages of scrapie-infected mice were substantially more than those of mid-late and terminal stages. More DEAPs were observed in the samples of ME7- than 139A-infected mice. In the 80 dpi samples, 99 (98%) out of 101 DEAPs in ME7 and 30 (96.8%) out of 31 DEAPs in 139A were down-regulated. In the 120 dpi samples,
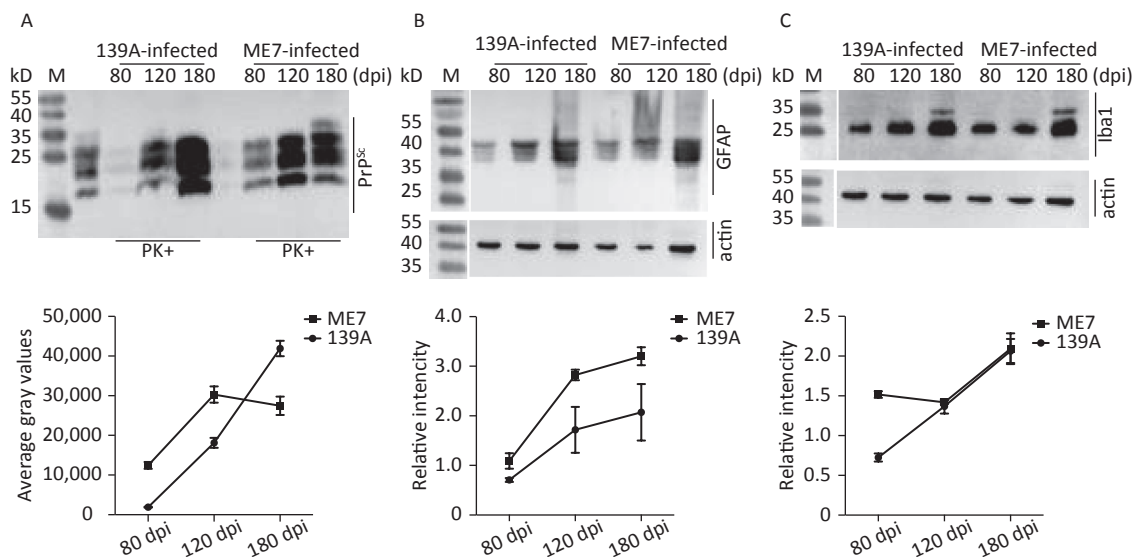
Figure 1. Western blot evaluations of PrP^Sc, GFAP, and Iba1 in the brain tissues of 139A- and ME7-infected mice collected at mid-early, mid-late, and terminal stages. The brain homogenates from three individual infected mice collected at different time points were pooled and used as the representative samples. (A) PK-digested Western blot. (B) GFAP-specific Western blot. (C) Iba1-specific Western blot. Quantitative assays of the average intensities of the target bands are shown at the bottom of individual representative images. The relative intensities of GFAP and Ibal were normalized with the data of individual actin.

		139A-180	139A-120	139A-80	ME7-180	ME7-120	ME7-80
decreased	> 1.5 fold	8	7	104	54	39	366
increased	> 1.5 fold	43	35	14	21	188	24

	139A-180	139A-120	139A-80	ME7-180	ME7-120	ME7-80
> 2.0 fold	1	0	7	8	3	86
> 2.0 fold	5	5	1	4	33	5

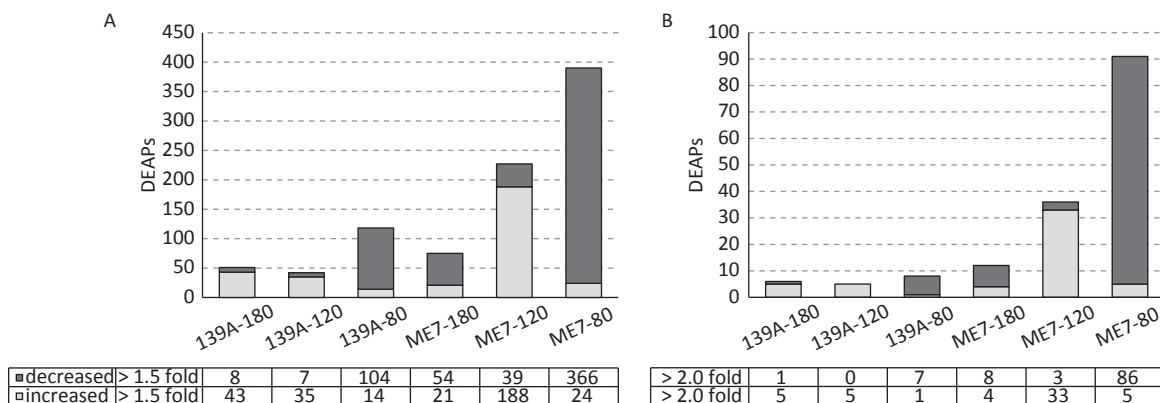**Figure 2.** Numbers of DEAP in the brains of 139A- and ME7-infected mice collected at mid-early, mid-late, and terminal stages. (A) Based on a 1.5-fold change. (B) Based on a 2.0-fold change. The numbers of increased and decreased DEAPs in each sample are shown at the bottom.

the decreased DEAPs were reduced to 15.9% (7/44) in ME7 and 54.5% (6/11) in 139A. In the late stage samples (180 dpi), all four DEAPs in 139A increased, whereas 3 (21%) out of 14 DEAPs in ME7 showed increases.

Further, the consistency and dissimilarity of the mitochondrial associated DEAPs at each time point between two scrapie-infected mice were analyzed. The acetylated peptides showing differential expression in two scrapie experimental mice were considered overlapping. The acetylated peptides showing differential expression in one infected model but not differentially expressed while expressed at the same tendency (> 1.5 and < 1.0 for the increased ones and > 1.0 and < 0.666 for the decreased ones) in another model were considered as consistent ones. The acetylated peptides showing differential expression in one infected model but were expressed at the opposite tendency were considered dissimilar ones. As shown in Figure 3B, in the mid-early stage samples, 29 acetylated peptides overlapped, 73 were consistent, and none were dissimilar between 139A- and ME7-infected mice. In the samples for the mid-late stage, 6 were overlapped, 37 were consistent, and 4 were dissimilar. In the late stage samples, no acetylated peptides overlapped, but 17 were consistent, and 1 was dissimilar. This finding indicates that the predominantly majority of the identified acetylated mitochondrial associated peptides were consistently expressed in the brains of the two kinds of scrapie-infected mice at three time points during infection, although the samples of ME7-infected mice contained notably more DEAPs than 139A-infected ones.

The bioinformatic assay revealed that 328 identified acetylated mitochondrial associated peptides belonged to 74 different proteins, with 44 (59.5%) proteins showing differential expression in at least one tested time point. The names of these 44 proteins, the numbers of the identified peptides, the numbers of DEAPs, the acetylated positions of the individual differentially expressed proteins (DEPs), and the DEAPs in the tested samples were summarized in (Supplementary Table S1 available in www.besjournal.com). A total of 9 (20.5%) out of 44 proteins contained 10 or more than 10 identified peptides, including aconitate hydratase (with 6 DEAPs), aspartate aminotransferase (with 14 DEAPs), ATP synthase subunit alpha (with 8 DEAPs), ATP synthase subunit beta (with 5 DEAPs), dihydrolipoyl dehydrogenase (with 6 DEAPs), glutamate dehydrogenase 1 (with 12 DEAPs), isocitrate dehydrogenase [NADP] (with 2 DEAPs), malate dehydrogenase (with 8 DEAPs), and pyruvate dehydrogenase E1 component subunit alpha (with 8 DEAPs). In addition, 24 (54.5%) differentially changed proteins contained 2–9 identified peptides, and 11 (25%) proteins contained one identified peptide.

Three up-regulated DEAPs were identified in the mid-early stage samples, two in ME7-infected and one in 139A-infected mice. All three up-regulated DEAPs belonged to ATP synthase subunit alpha, and the acetylated sites were at aa.194 (for ME7 and 139A) and aa.541 (for ME7). Further analysis revealed that the level of the acetylated peptide at aa.541 in the 139A-80 dpi sample exhibited a 1.4675-fold increase. The two acetylated peptides returned to normal ranges in the 120 and 180 dpi

A	Mitochondrial OS					
	139A-180	139A-120	139A-80	ME7-180	ME7-120	ME7-80
decreased	0	6	30	11	7	99
increased	4	5	1	3	37	2

B	Mitochondrial OS		
	80 dpi	120 dpi	180 dpi
dissimilar	0	4	1
consistent	73	37	17
overlapped	29	6	0

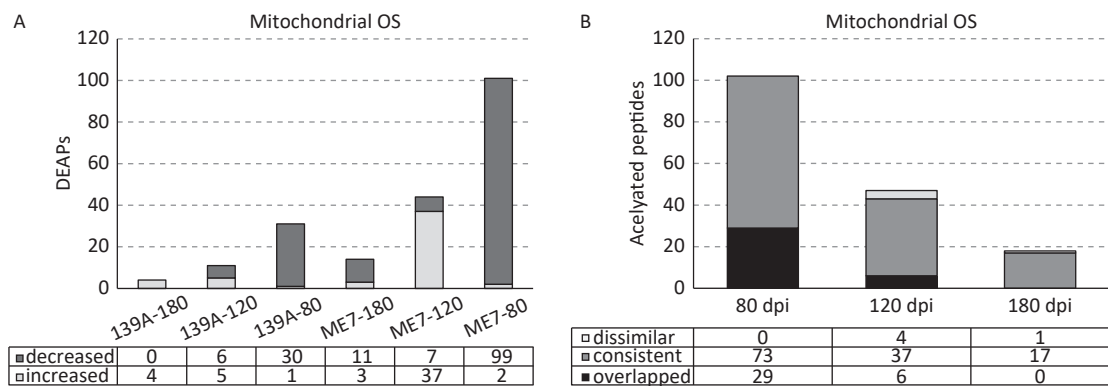**Figure 3.** Mitochondrial associated DEAPs in the brains of 139A- and ME7-infected mice collected at mid-early, mid-late, and terminal stages. (A) Numbers of DEAPs based on 1.5-fold change. The numbers of increased and decreased DEAPs in each sample are shown at the bottom. (B) Change trends of DEAPs. The numbers of overlapping, similar, and dissimilar DEAPs in each sample are shown at the bottom.

samples of ME7- and 139A-infected mice. Seven down-regulated DEAPs in the 80 dpi samples were significantly up-regulated in the 120 dpi samples. These DEAPs were acyl-coenzyme A thioesterase 2 acetylated at aa.83, acyl-coenzyme A thioesterase 9 acetylated at aa.102, dihydrolipoyl dehydrogenase acetylated at aa.122, dihydrolipoyllysine-residue succinyltransferase component of 2-oxoglutarate dehydrogenase complex acetylated at aa.268, isocitrate dehydrogenase [NAD] subunit alpha acetylated at aa.200 and aa.214, peptidyl-prolyl cis-trans isomerase F acetylated at aa.85, pyruvate dehydrogenase E1 component subunit alpha acetylated at aa.244 and 313, and succinate--CoA ligase [ADP-forming] subunit beta acetylated at aa.88. In parallel, 79 down-regulated DEAPs in the 80 dpi samples were normal ranges in 120 and 180 dpi samples, with the majority showing increasing trends in 120 dpi and decreasing slightly in 180 dpi. Twelve down-regulated DEAPs in the 80 dpi samples remained significantly down-regulated in the subsequent samples. In the 120 dpi samples, 26 DEAPs were up-regulated only at this time point, 7 up-regulated ones were down-regulated significantly in 80 dpi samples, and 6 up-regulated ones maintained their increased status in 180 dpi samples. In addition, all 11 down-regulated and 7 up-regulated DEAPs in the 180 dpi samples were identified as DEAPs in 80 and/or 120 dpi samples. These data indicated that during scrapie infection, the acetylation of the mitochondrial related proteins in the whole brain tissues is markedly down-regulated in the mid-early stage, becomes active in the mid-late stage, and turns relatively silent in the terminal stage.

Involvement of Significant Pathways in the Brain Samples of 139A- and ME7-infected Mice Collected at the Mid-early, Mid-late, and Terminal Stages

To analyze the possible involved biological pathway of the DEAPs, the Kyoto Encyclopedia of Genes and Genomes (KEGG) pathway analysis was conducted using the KOBAS2.0 software. As shown in Figure 4A, 55, 25, and 18; and 39, 13, and 10 biological pathways were significantly changed ($P <$ 0.05) in the 80, 120, and 180 dpi samples of ME7- and 139A-infected mice, respectively. The top 10 involved pathways based on their *P* values, and the numbers of DEAPs in each tested sample were summarized in (Supplementary Table S2 available in www.besjournal.com). Six significantly changed biological pathways were identified in all tested samples, including carbon metabolism, metabolic pathways, biosynthesis of amino acids, glycolysis/gluconeogenesis, pyruvate metabolism, and citrate cycle (TCA cycle). Subsequently, the numbers of the involved up- and down-regulated DEAPs in these six pathways for each tested sample were counted (Figure 4B–4G). All six pathways showed similar distribution patterns of DEAPs, with predominantly down-regulated DEAPs in the mid-early stage and up-regulated DEAPs in the mid-late and late stages. Meanwhile, the numbers of involved DEAPs in these pathways reduced along with the incubation, particularly in the brain samples of ME7-infected mice. Two kinds of scrapie-infected mice models also displayed other differences besides the numbers of involved DEAPs. In the samples of 139A-infected mice, all DEAPs involved in the six pathways were down-regulated in 80 dpi and up-regulated in 180 dpi samples. In the 120 dpi samples, the DEAPs in three pathways were all up-regulated, and the other three contained one down-regulated DEAP. A similar pattern was also observed in the samples of ME7-infected mice, with an overwhelming majority of down-regulated DEAPs observed in the 80 dpi samples and the majority of up-regulated DEAPs found in 120 dpi samples. In the 180 dpi samples, the numbers of DEAPs were considerably less, and the ratios of up- and down-regulated DEAPs in most (5/6) involved pathways were almost the same.

Changes in the Involved DEAPs in the Citrate Cycle (TCA cycle) Pathway in the Brain Samples of 139A- and ME7-infected Mice Collected at the Mid-early, Mid-late, and Terminal Stages

The citrate cycle or TCA cycle, which is located in the cytoplasm of prokaryotes and mitochondria of eukaryotes, is an essential metabolism pathway in the aerobic body. The acetylation processes of dozens of enzymes in the TCA cycle showed significant changes in the brain tissues during prion infections, covering 13 and 8 down-regulated DEAPs in 80 dpi samples, 8 and 2 up-regulated ones in 120 dpi samples, 3 and 2 up-regulated ones in 180 dpi samples of ME7- and 139A-infected mice, respectively (Figure 4C). Furthermore, the status of each DEAP at the three time points was analyzed (Supplementary Table S3 available in www. besjournal.com). A total of 7 out of 8 down-regulated DEAPs in 80 dpi samples of 139A-infected mice significantly decreased compared with that of ME7-infected mice. The rest of the involved DEAPs observed in one type of scrapie-infected mouse (5 in ME7 and 1 in 139A) also showed down-regulated tendencies in another model despite the
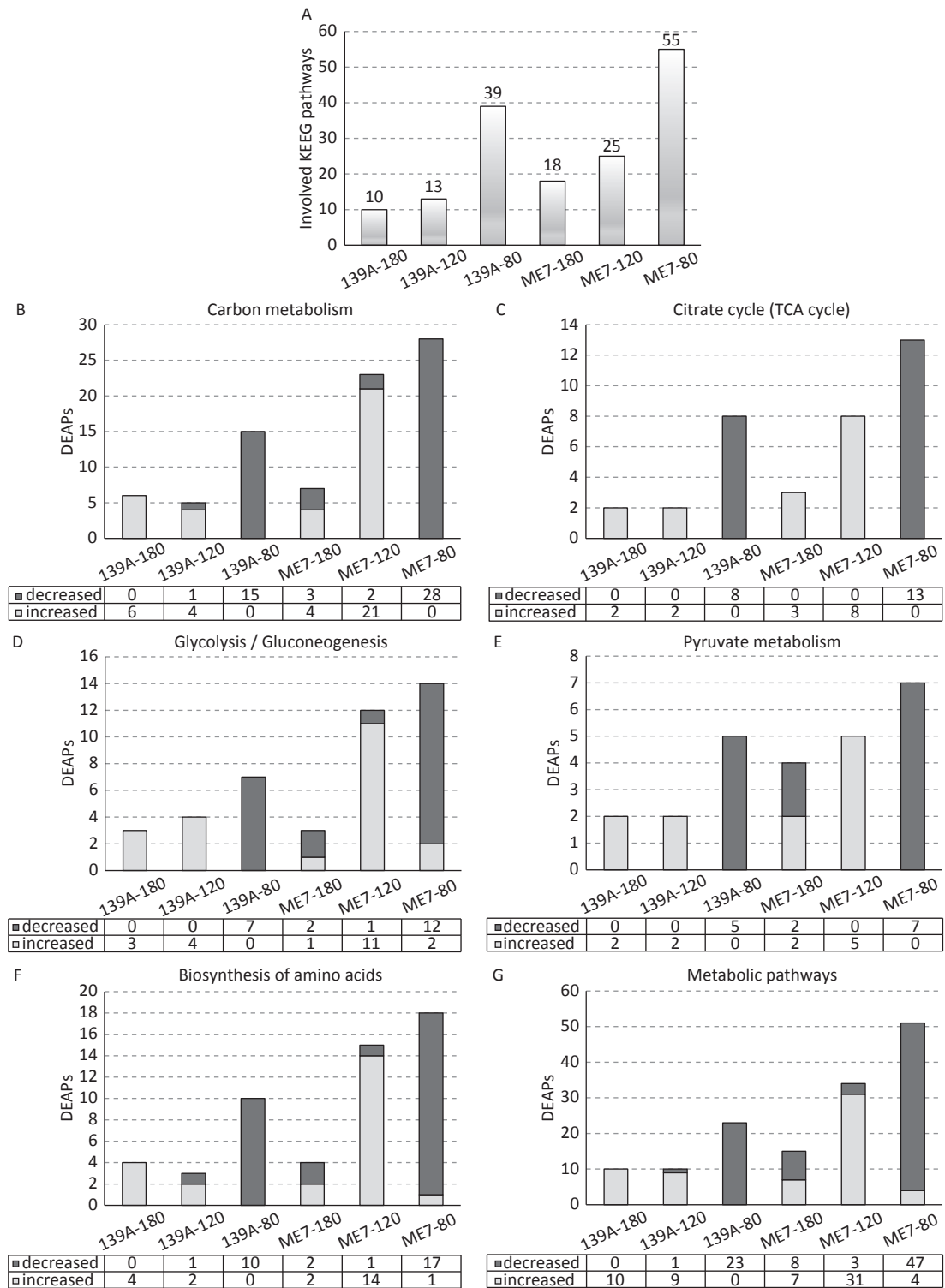
Figure 4. Numbers of involved KEGG pathways and DEAPs in six commonly detected pathways in the brains of 139A- and ME7-infected mice collected at mid-early, mid-late, and terminal stages. (A) KEGG pathways. The numbers of involved pathways in each sample are indicated at the top. (B) Carbon metabolism. (C) TCA cycle. (D) Glycolysis/Gluconeogenesis. (E) Pyruvate metabolism. (F) Biosynthesis of amino acids. (G) Metabolic pathways. The numbers of increased and decreased DEAPs in each sample are shown at the bottom.

insignificance. Most of these down-regulated DEAPs increased in the 120 dpi samples, with 4 DEAPs being significantly up-regulated. All down-regulated DEAPs in the 80 dpi samples dropped to the normal ranges in 180 dpi samples. All eight DEAPs in the TCA cycle identified in the 120 dpi samples were up-regulated, and among them, two DEAPs were commonly detected in 139A- and ME7-infected mice. A total of 3 out of 8 up-regulated DEAPs in the 120 dpi samples maintained their increases, and another 5 returned to normal ranges in the 180 dpi samples. In the 180 dpi samples, 4 DEAPs were identified in the TCA cycle, and all of them were up-regulated. These data strongly indicated that the acetylating processes of the enzymes of the TCA cycle in the brain tissues were negatively regulated in the early stage and positively regulated in the mid-late and terminal stages of prion infection.

The potentially affected steps in the TCA cycle due to changes in the DEAPs in the brain tissues at different time points during prion infection were evaluated. Dozens of steps in the TCA cycle were affected *via* negatively regulated acetylation for relevant enzymes in the 80 dpi samples (left panels in Figure 5A and 5B). Many steps were also affected in the 120 dpi samples *via* the up-regulated acetylation for the enzymes, particularly in ME7-infected mice (middle panels in Figure 5A and 5B). In the 180 dpi samples, the affected steps focused on the processes from succinate to fumarate, fumarate to malate, and malate to oxaloacetate *via* positively regulated acetylation for succinate dehydrogenase, fumarate hydratase, and malate dehydrogenase (right panels in Figure 5A and 5B). Thus, the activity of the TCA cycle in the context of the whole brain is strongly influenced by deacetylation in the early stage and by acetylation in the mid-late and late stages during prion infection.

DISCUSSION

In this study, we screened the global acetylation situations of the brain proteins of two scrapie-infected mouse models at the mid-early, mid-late, and terminal stages using an advanced proteomic technique. The potential involved in biological functions and pathways due to alterations in protein acetylation were analyzed. A total of 1,485 acetylated peptides in the brain tissues of the mouse have been identified, and hundreds of them showed differential expression, with either a 1.5-fold increase or decrease at various time points during scrapie infection. To our knowledge, this research is the first comprehensive description of the global protein acetylation in brain tissues during prion infection.

Two scrapie-infected mouse models showed similar alterative patterns of the global acetylating profiles of the whole brain proteins during infection despite the difference in the numbers of DEAPs. In the brains at the mid-early stage (80 dpi), markedly higher numbers of DEAPs were observed, and the absolute majority displayed down-regulation. In the mid-late (120 dpi) and terminal (180 dpi) stages, the numbers of DEAPs were reduced, and large portions of them were up-regulated. The alterative tendencies of the brain protein acetylated profiles during prion infection were completely different from the changes in the global profiles of brain proteins from the two scrapie-infected mouse models[8]. In the proteomic study, considerably more DEPs were observed in the terminal stage samples (180 dpi) than in the mid-late stage (80 dpi)[8]. This result implies that brain protein acetylation situations are reversible during prion infection because more DEAPs were markedly observed in the mid-early (80 dpi) and close to normal in the mid-late (120 dpi) and terminal (180 dpi) stages.

The majority of DEAPs during prion infection are involved in the enzymatic proteins participating in various metabolism activities. The analyses of the involved KEGG pathways also revealed the same feature. Large portions of the involved pathways are associated with the metabolism, e.g., carbon metabolism, metabolic pathways, glyoxylate and dicarboxylate metabolism, pyruvate metabolism, TCA cycle, etc. However, in the assays of global brain proteomics for 139A- and ME7-infected mice[8] and for different subtypes of human prion diseases[6], the most frequently involved pathways are the ones related to inflammation, e.g., complement and coagulation cascades, *Staphylococcus aureus* infection, Chagas disease (*American trypanosomiasis*), Leishmaniasis, systemic lupus erythematosus, etc., in which up-regulation of some complement components (C1q, C2, C3, and C4) are commonly addressed. The diversity of the involved pathways addressed by two types of proteomic assays reflects two different aspects of the whole proteins in the brains infected with prions.

Mitochondria are the sites of oxidative metabolism in eukaryotes, where sugars, fats, and amino acids eventually oxidize and release energy[26]. Our data here revealed that approximately 1/3 of identified acetylated peptides were marked as mitochondrial OS, and more than 40% of

139A-infected mice

ME7-infectedmice

A   80 dpi

B   80 dpi

120 dpi

120 dpi

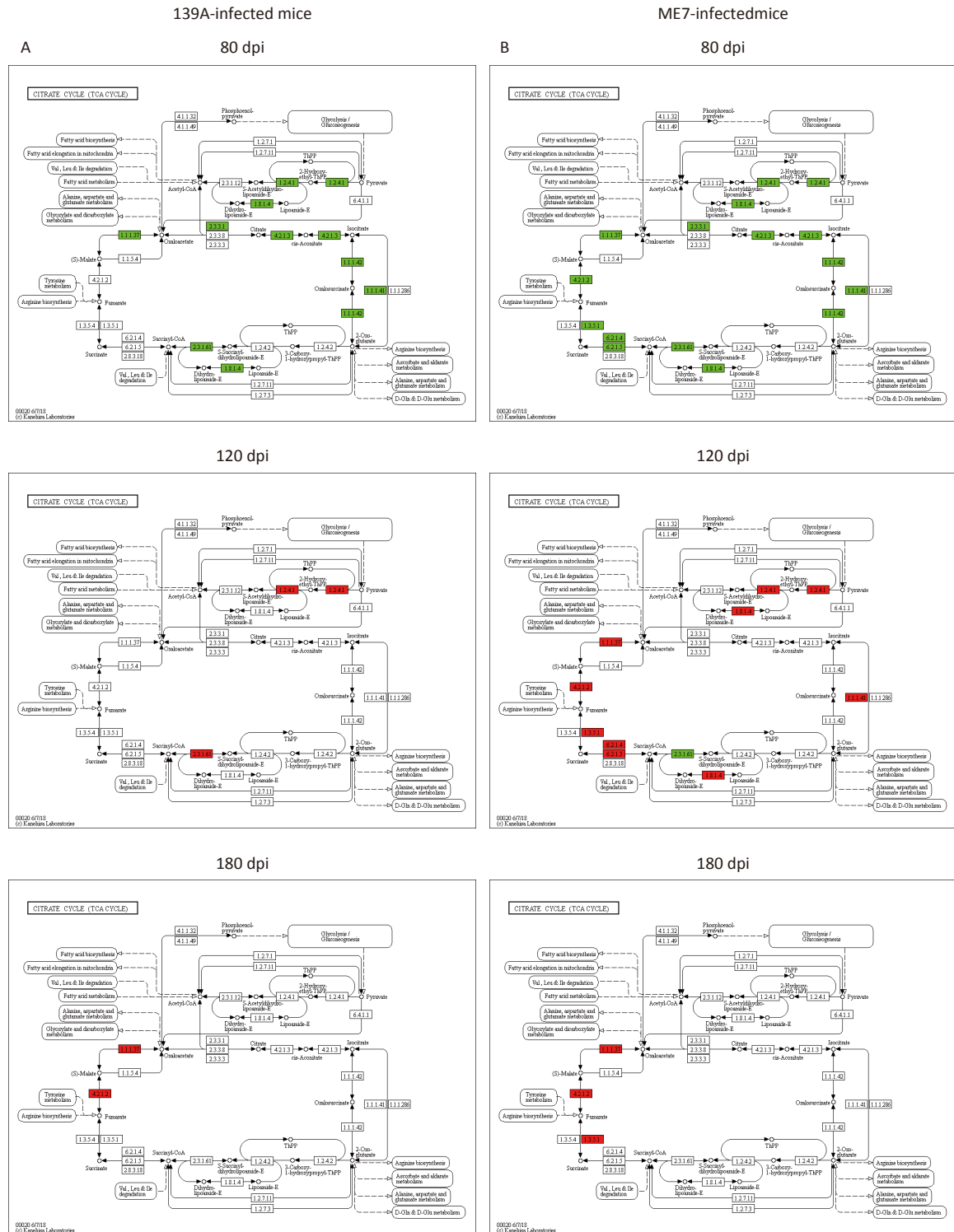180 dpi

180 dpi

Figure 5. Analysis of up- or down-regulated acetylated proteins (enzymes) and catalytic steps in the pathway of the TCA cycle in the brains of 139A- and ME7-infected mice collected at mid-early, mid-late, and terminal stages. (A) 139A-infected mice (B) ME7-infected mice. Down-regulated acetylated enzymes are marked in green, and up-regulated ones are marked in red.

mitochondrial associated acetylated peptides were DEAPs. Despite the difference in the numbers of DEAPs, the two scrapie-infected mouse models showed similar alterative patterns of mitochondrial associated DEAPs during infection; that is, the vast majority of down-regulated DEAPs were in the mid-early stage, but more ratios of up-regulated DEAPs were recorded in the mid-late and terminal stages. Moreover, the overwhelming majority of the identified brain mitochondrial associated DEAPs in the two scrapie mouse models revealed the same change tendency during the infection. The mitochondrial associated DEAPs subsequently induced significant changes in a series of pathways. Six significantly changed pathways identified in all tested samples contained the processes within mitochondria. Notably, the brain mitochondrial functions were influenced by protein deacetylation (in the early and mid-early stages) and acetylation (in the mid-late and terminal stages) during prion infection.

The TCA cycle is an essential metabolic pathway in aerobic organisms. It is the final metabolic pathway of the three major nutrients and the junction of the metabolism of sugars, lipids, and amino acids[27]. The TCA cycle occurs within the matrix of the mitochondrion, which contains eight enzymatic steps, including those for citrate synthase, aconitate hydratase, isocitrate dehydrogenase, oxoglutarate dehydrogenase, succinate--CoA ligase, succinate dehydrogenase, fumarate hydratase, and malate dehydrogenase[28]. In the mid-early stage, all eight enzymes were deacetylated. However, in the mid-late stage, six enzymes (isocitrate dehydrogenase, oxoglutarate dehydrogenase, succinate--CoA ligase, succinate dehydrogenase, fumarate hydratase, and malate dehydrogenase) in the sample of ME7-infected mice and one (oxoglutarate dehydrogenase) in 139A-infected ones were significantly acetylated, and the rests were in normal levels. In the late stage, three enzymes (succinate dehydrogenase, fumarate hydratase, and malate dehydrogenase) in ME7-infected mice and two (fumarate hydratase and malate dehydrogenase) in 139A-infected ones are in the status of acetylation. The alteration and reversion of the acetylation and deacetylation of almost all enzymes in TCA cycle may reflect the changes in the activity of this pathway in the brains during prion infection. As the core process linked with the metabolism of carbohydrates, fats, and proteins[28,29], changes in the TCA cycle will definitely affect the other metabolic pathways.

Although histone acetylation has played a critical role in chromatin remodeling for a long time[30-32], the functional roles of acetylation in the vast majority of thousands of non-histone proteins are still unclear. Advances in MS-based proteomics proposed a vast of acetylated proteins involved in metabolic pathways in eukaryotes and bacteria, such as glycolysis and the TCA cycle[16,33]. By performing proteomic analysis of 48 phylogenetically distant bacteria, Choudhary and colleagues reported that lysine acetylation occurs in evolutionarily conserved lysine residues in catalytic sites of enzymes involved in central carbon metabolism and plays a direct role in metabolic regulation by switching off the enzyme activity[34]. ApoE-deficient C57Bl/6J mice exposed to low-dose-rate gamma radiation showed that the great majority of the hyperacetylated proteins are involved in the TCA cycle, fatty acid oxidation, oxidative stress response, and sirtuin pathway, which is associated with impairment of heart metabolism[35]. Although the direct evidence to support the association of enzymic acetylation with the functions of metabolic pathways in the brains of prion diseases is still lacking, the hyperacetylation of enzymes in the TCA cycle may be a negative regulator for enzymatic activity, and deacetylation may benefit the TCA cycle. Further assays addressing the association between acetylation status and enzymatic activity in metabolic pathways, e.g., TCA cycle, during prion infection are mostly deserved.

The process of protein acetylation and deacetylation is a reversible post-translation modification in regulating cellular function and response to external stimuli[15,36]. The data here also illustrated the reversible alteration of brain protein acetylation during prion infection. However, the changes in protein acetylation in this study reflect the alteration in the context of whole brain tissues. Similar changing profiles were also observed in the brain levels of nitric oxide, nitric oxide synthase, and S-nitrosylation of several proteins, e.g., aquaporin-1, calcium/calmodulin-dependent protein kinase II, neurogranin, and opalin in several experimental scrapie-infected rodents[37]. The exact reason for the reversible alteration of brain protein acetylation during prion infection is unclear. One possibility is the association with the changes in deacetylases, such as the sirtuin pathway, in the brains during prion infection. Our previous studies have shown that in addition to marked declines of brain Sirt1 and Sirt3 at the terminal stage of different prion diseases; the brain level of Sirt1 in the scrapie agent 263K-infected hamsters maintained a high level in

the early stage, dropped down in the mid-late stage, and continually decreased until the end stage[19]. Another possibility is related to the gradual appearance of neuropathological abnormalities, such as PrP^Sc deposit, astrogliosis, and activated microglia in the brain tissues. Our data here and in other previous studies[8,38,39] demonstrated that the amounts of PrP^Sc in the samples of the mid-early stage (80 dpi) were remarkably less than in those of samples from the mid-late (120 dpi) and end (180 dpi) stages of the two scrapie-infected mouse models. Meanwhile, significant increases in GFAP- and Iba1-signals were also detected since the mid-late stage. Notably, the marked neuropathological changes occurred since the mid-late stage. In such a case, we may assume that in the early stage of prion infection with less PrP^Sc deposit and reactive gliosis, the host brain can maintain biological functions to overcome the neurotoxicity produced by prion infection, at least partially, *via* deacetylation of enzymes associated with various metabolic pathways. Along with the increased PrP^Sc deposit and severe reactive inflammation in the CNS tissues in the late stage, the deacetylation process may be inhibited, for example, due to declined levels of the sirtuin pathway in the brain, which is likely to contribute to the impairment of mitochondrial function.

In addition, the evaluation of protein acetylation during prion infection in this study refers to the global changes in whole brain tissues that contain not only damaged neurons but also proliferative astrocytes and activated microglia. We cannot simply conclude whether such alteration is due to the accumulation of aggregated proteins or due to subsequently reactive inflammation. We were also unable to distinguish the defined changes in protein acetylation in damaged neurons, proliferative astrocytes, and activated microglia. These questions deserve further exploration.

CONCLUSIONS

In conclusion, our data here illustrated a view of the global acetylation for brain proteins during prion infection, showing remarkably inhibiting acetylation in the early stage and relatively enhanced acetylation in the late stage. In the late stage, the affected steps focused on up-regulated acetylation for succinate dehydrogenase, fumarate hydratase, and malate dehydrogenase. This finding possibly reflects the host (brain) response to external prions to overcome the neurotoxicity in the early stage and

the impairment of metabolic and mitochondrial functions due to PrP^Sc deposit and reactive inflammation.

REFERENCES

1. Chen C, Dong XP. Epidemiological characteristics of human prion diseases. Infect Dis Poverty, 2016; 5, 47.
2. Shi Q, Xie WL, Zhang BY, et al. Brain microglia were activated in sporadic CJD but almost unchanged in fatal familial insomnia and G114V genetic CJD. Virol J, 2013; 10, 216.
3. Lv Y, Chen C, Zhang BY, et al. Remarkable activation of the complement system and aberrant neuronal localization of the membrane attack complex in the brain tissues of scrapie-infected rodents. Mol Neurobiol, 2015; 52, 1165–79.
4. Xu Y, Tian C, Sun J, et al. FBXW7-induced MTOR degradation forces autophagy to counteract persistent prion infection. Mol Neurobiol, 2016; 53, 706–19.
5. Xu Y, Tian C, Wang SB, et al. Activation of the macroautophagic system in scrapie-infected experimental animals and human genetic prion diseases. Autophagy, 2012; 8, 1604–20.
6. Shi Q, Chen LN, Zhang BY, et al. Proteomics analyses for the global proteins in the brain tissues of different human prion diseases. Mol Cell Proteomics, 2015; 14, 854–69.
7. Tian C, Liu D, Chen C, et al. Global transcriptional profiling of the postmortem brain of a patient with G114V genetic Creutzfeldt-Jakob disease. Int J Mol Med, 2013; 31, 676–88.
8. Shi Q, Chen LN, Lv Y, et al. Comparative proteomics analyses for 139A and ME7 scrapie infected mice brains in the middle and terminal stages. Proteomics Clin Appl, 2017; 11, 1600113.
9. Voet S, Srinivasan S, Lamkanfi M, et al. Inflammasomes in neuroinflammatory and neurodegenerative diseases. EMBO Mol Med, 2019; 11, e10248.
10. Chen LN, Shi Q, Zhang BY, et al. Proteomic analyses for the global S-nitrosylated proteins in the brain tissues of different human prion diseases. Mol Neurobiol, 2016; 53, 5079–96.
11. Katsumoto A, Takeuchi H, Tanaka F. Tau pathology in chronic traumatic encephalopathy and alzheimer's disease: similarities and differences. Front Neurol, 2019; 10, 980.
12. Alonso AD, Cohen LS, Corbo C, et al. Hyperphosphorylation of Tau associates with changes in its function beyond microtubule stability. Front Cell Neurosci, 2018; 12, 338.
13. Ansari SA, Emerald BS. The role of insulin resistance and protein O-GlcNAcylation in neurodegeneration. Front Neurosci, 2019; 13, 473.
14. Sterner DE, Berger SL. Acetylation of histones and transcription-related factors. Microbiol Mol Biol Rev, 2000; 64, 435–59.
15. Yang XJ, Seto E. Lysine acetylation: codified crosstalk with other posttranslational modifications. Mol Cell, 2008; 31, 449–61.
16. Choudhary C, Kumar C, Gnad F, et al. Lysine acetylation targets protein complexes and co-regulates major cellular functions. Science, 2009; 325, 834–40.
17. Deng WK, Wang CW, Zhang Y, et al. GPS-PAIL: prediction of lysine acetyltransferase-specific modification sites from protein sequences. Sci Rep, 2016; 6, 39787.
18. Carrico C, Meyer JG, He WJ, et al. The mitochondrial acylome emerges: proteomics, regulation by sirtuins, and metabolic

and disease implications. Cell Metab, 2018; 27, 497−512.

19. Wang J, Zhang J, Shi Q, et al. Scrapie infection in experimental rodents and SMB-S15 cells decreased the brain endogenous levels and activities of Sirt1. J Mol Neurosci, 2015; 55, 1022−30.

20. Maimaitiming A, Xiao K, Hu C, et al. Aberrant decrease of the endogenous SIRT3 and increases of acetylated proteins in scrapie-infected cell line SMB-S15 and in the brains of experimental mice. ACS Chem Neurosci, 2019; 10, 4293−302.

21. Sonawane SK, Chinnathambi S. Prion-like propagation of post-translationally modified Tau in Alzheimer's disease: a hypothesis. J Mol Neurosci, 2018; 65, 480−90.

22. Phadwal K, Kurian D, Salamat MKF, et al. Spermine increases acetylation of tubulins and facilitates autophagic degradation of prion aggregates. Sci Rep, 2018; 8, 10004.

23. Rasouli S, Abdolvahabi A, Croom CM, et al. Lysine acylation in superoxide dismutase-1 electrostatically inhibits formation of fibrils with prion-like seeding. J Biol Chem, 2017; 292, 19366−80.

24. Xiao K, Zhang BY, Zhang XM, et al. Re-infection of the prion from the scrapie-infected cell line SMB-S15 in three strains of mice, CD1, C57BL/6 and Balb/c. Int J Mol Med, 2016; 37, 716−26.

25. Chen Z, Wen B, Wang QH, et al. Quantitative proteomics reveals the temperature-dependent proteins encoded by a series of cluster genes in *Thermoanaerobacter tengcongensis*. Mol Cell Proteomics, 2013; 12, 2266−77.

26. Glancy B. Visualizing mitochondrial form and function within the cell. Trends Mol Med, 2020; 26, 58−70.

27. Murphy MP, O'Neill LAJ. Krebs cycle reimagined: the emerging roles of succinate and itaconate as signal transducers. Cell, 2018; 174, 780−4.

28. Van Der Bliek AM, Sedensky MM, Morgan PG. Cell biology of the mitochondrion. Genetics, 2017; 207, 843−71.

29. Altman BJ, Stine ZE, Dang CV. From Krebs to clinic: glutamine metabolism to cancer therapy. Nat Rev Cancer, 2016; 16, 619−34.

30. Hebbes TR, Thorne AW, Crane-Robinson C. A direct link between core histone acetylation and transcriptionally active chromatin. EMBO J, 1988; 7, 1395−402.

31. Cabot B, Cabot RA. Chromatin remodeling in mammalian embryos. Reproduction, 2018; 155, R147−58.

32. Kim S, Kaang BK. Epigenetic regulation and chromatin remodeling in learning and memory. Exp Mol Med, 2017; 49, e281.

33. Zhao SM, Xu W, Jiang WQ, et al. Regulation of cellular metabolism by protein lysine acetylation. Science, 2010; 327, 1000−4.

34. Nakayasu ES, Burnet MC, Walukiewicz HE, et al. Ancient regulatory role of lysine acetylation in central metabolism. mBio, 2017; 8, e01894−17.

35. Barjaktarovic Z, Merl-Pham J, Braga-Tanaka I, et al. Hyperacetylation of cardiac mitochondrial proteins is associated with metabolic impairment and sirtuin downregulation after chronic total body irradiation of ApoE$^{-/-}$ mice. Int J Mol Sci, 2019; 20, 5239.

36. Santo-Domingo J, Dayon L, Wiederkehr A. Protein lysine acetylation: grease or sand in the gears of β-cell mitochondria? J Mol Biol, 2020; 432, 1446-60.

37. Chen LN, Sun J, Yang XD, et al. The brain NO levels and NOS activities ascended in the early and middle stages and descended in the terminal stage in scrapie-infected animal models. Mol Neurobiol, 2017; 54, 1786−96.

38. Shi Q, Zhang BY, Gao C, et al. Mouse-adapted scrapie strains 139A and ME7 overcome species barrier to induce experimental scrapie in hamsters and changed their pathogenic features. Virol J, 2012; 9, 63.

39. Chen C, Xu XF, Zhang RQ, et al. Remarkable increases of α1-antichymotrypsin in brain tissues of rodents during prion infection. Prion, 2017; 11, 338−51.

Supplementary Table S1. The differentially changed mitochondrial associated proteins in in the brain samples of 139A- and ME7-infected mice collected at mid-early (80 dpi), mid-late (120 dpi) and terminal (180 dpi) stages

	Protein	No. of identified peptide	No. of DEAP	Acetylated position (down)	Changed in sample (No. of DEAP)	Acetylated position (up)	Changed in sample (No. of DEAP)
1	28S ribosomal protein S9	1	1	aa. 28	ME7 80 dpi (1)	/	/
2	4-aminobutyrate aminotransferase	4	1	aa. 400	ME7 80 dpi (1)	/	/
3	60 kD heat shock protein	2	1	aa. 130	ME7 80 dpi (1), 139A 80 dpi (1), ME7 180 dpi (1)	/	/
4	Aconitate hydratase	20	6	aa. 50, 168, 517, 736, 743	ME7 80 dpi (6), 139A 80 dpi (1)	/	/
5	Acyl-coenzyme A thioesterase 2	1	1	aa. 83	ME7 80 dpi (1)	aa. 83	ME7 120 dpi (1), 139A 120 dpi (1)
6	Acyl-coenzyme A thioesterase 9	4	3	aa. 102, 155	ME7 80 dpi (3), 139A 80 dpi (1)	aa. 102	ME7 120 dpi (1)
7	Aspartate aminotransferase	29	14	aa. 73, 82, 94, 122, 159, 363, 404	ME7 80 dpi (11), 139A 80 dpi (5), ME7 120 dpi (1), 139A 120 dpi (3), ME7 180 dpi (3)	aa. 73, 404	ME7 120 dpi (4)
8	ATP synthase F(0) complex subunit B1	9	3	aa. 162, 225, 233	ME7 120 dpi (1), 139A 80 dpi (1), 139A 120 dpi (1), ME7 180 dpi (2)	/	/
9	ATP synthase subunit alpha	20	8	aa. 126, 261, 498, 539	ME7 80 dpi (4), 139A 80 dpi (1)	aa. 194, 230, 498, 541	ME7 80 dpi (2), 139A 80 dpi (1), ME7 120 dpi (2), ME7 180 dpi (1)
10	ATP synthase subunit beta	11	5	aa. 212	ME7 120 dpi (2)	aa. 426, 259	ME7 (3)
11	ATP synthase subunit d	7	2	aa. 73, 117	ME7 80 dpi (2)	/	/
12	Calcium uniporter protein	2	1	aa. 331	ME7 80 dpi (1)	/	/
13	Citrate synthase	5	4	aa. 237, 366, 370	ME7 80 dpi (4), 139A 80 dpi (2)	/	/
14	Cytochrome b-c1 complex subunit 2	3	2	aa. 92, 250	ME7 80 dpi (2), 139A 80 dpi (1), ME7 180 dpi (1)	/	/
15	Cytochrome c1	1	1	/	ME7 80 dpi (1)	/	/
16	Dihydrolipoyl dehydrogenase	14	6	aa. 122, 401	ME7 80 dpi (5), 139A 80 dpi (1)	aa. 122, 420	ME7 120 dpi (2)
17	Dihydrolipoyllysine-residue succinyltransferase component of 2-oxoglutarate dehydrogenase complex	3	3	aa. 268, 274	ME7 80 dpi (2), 139A 80 dpi (1), ME7 120 dpi (1)	aa. 268	ME7 120 dpi (1), 139A 120 dpi (1)
18	Electron transfer flavoprotein subunit alpha	5	2	aa. 69	ME7 80 dpi (2)	/	/
19	ES1 protein homolog	3	1	aa. 231	ME7 80 dpi (1), 139A 80 dpi (1), ME7 180 dpi (1)	/	/
20	Fumarate hydratase	8	4	aa. 77	ME 80 dpi (1)	aa. 63, 227	ME7 120 dpi (2), ME7 180 (1), 139A 180 dpi (1)
21	Glutamate dehydrogenase 1	12	4	aa. 84, 90, 527	ME7 80 dpi (3), 139A 80 dpi (2)	aa. 527	ME7 120 dpi (1)

Continued

	Protein	No. of identified peptide	No. of DEAP	Acetylated position (down)	Changed in sample (No. of DEAP)	Acetylated position (up)	Changed in sample (No. of DEAP)
22	Glutaminase kidney isoform	1	1	aa. 668	ME7 80 dpi (1)	/	/
23	Hydroxyacyl-coenzyme A dehydrogenase	3	1	aa. 157	ME7 80 dpi (1), 139A 80 dpi (1)	/	/
24	Isocitrate dehydrogenase [NAD] subunit alpha	9	8	aa. 200, 214, 326	ME7 80 dpi (5), 139A 80 dpi (1)	aa. 200, 214	ME7 120 dpi (5)
25	Isocitrate dehydrogenase [NAD] subunit	1	1	aa. 157	ME7 80 dpi (1)	/	/
26	Isocitrate dehydrogenase [NADP]	10	2	aa. 106,180	ME7 80 dpi (2)	/	/
27	Isovaleryl-CoA dehydrogenase	2	1	aa. 76	ME7 80 dpi (1)	/	/
28	Long-chain-specific acyl-CoA dehydrogenase	1	1	aa. 92	ME7 80 dpi (1)	/	/
29	Malate dehydrogenase	15	8	aa. 97, 297, 301, 307, 324, 338	ME7 80 dpi (8), 139A 80 dpi (1), ME7 180 dpi (1)	/	/
30	Methylglutaconyl-CoA hydratase	5	1	/	/	aa. 80	ME7 120 dpi (1)
31	Mitochondrial ATP synthase epsilon subunit	2	2	aa. 17, 26	ME7 80 dpi (2), ME7 180 (1)	/	/
32	Peptidyl-prolyl cis-trans isomerase F	1	1	/	/	aa. 85	ME7 120 dpi (1)
33	Persulfide dioxygenase ETHE1	1	1	aa. 66	ME7 80 dpi (1), 139A 80 dpi (1)	/	/
34	Presequence protease	4	2	/	/	aa. 305, 707	ME7 120 dpi (2), 139A 180 dpi (1)
35	Pyruvate dehydrogenase E1 component subunit alpha	10	8	aa. 85, 244, 313, 321	ME7 80 dpi (4), 139A 80 dpi (1)	aa. 63, 85, 244, 267, 313	ME7 120 dpi (6), 139A 120 dpi (1)
36	Pyruvate dehydrogenase E1 component subunit beta	2	1	aa. 354	ME7 80 dpi (1)	/	/
37	Pyruvate dehydrogenase protein X component	1	1	aa. 194	ME7 80 dpi (1)	/	/
38	Stress-70 protein	5	3	aa. 288, 612, 625	ME7 80 dpi (3), 139A 80 dpi (2)	/	/
39	Succinate dehydrogenase [ubiquinone] flavoprotein subunit	7	5	aa. 498, 550	ME7 80 dpi (4)	aa. 608	ME7 120 dpi (1), ME7 180 dpi (1)
40	Succinate--CoA ligase [ADP-forming] subunit beta	1	1	aa. 88	ME7 80 dpi (1)	aa. 88	ME7 120 dpi (1)
41	Succinate-semialdehyde dehydrogenase	2	1	aa. 128	ME7 80 dpi (1)	/	/
42	Superoxide dismutase [Mn]	9	6	aa. 68, 122	ME7 80 dpi (2), 139A 80 dpi (2), ME7 120 dpi (2), 130A 120 dpi (2), ME7 180 dpi (1)	aa. 68	ME7 120 dpi (1), 139A 120 dpi (2), 139A 180 dpi (1)
43	Trifunctional enzyme subunit alpha	8	4	aa. 60, 129, 353	ME7 80 dpi (3), 139A 80 dpi (1)	aa. 60	ME7 120 dpi (1), 139A 180 dpi (1)
44	Trifunctional enzyme subunit beta	1	1	/	/	aa. 333	ME7 120 dpi (1)

Supplementary Table S2. The top 10 involved pathways in the brain samples of 139A- and ME7-infected mice collected at mid-early (80 dpi), mid-late (120 dpi), and terminal (180 dpi) stages

| Brain sample	Involved pathway	*P* value	Acetylated Protein in Diff Exp
139A 180 dpi	Carbon metabolism - Mus musculus (mouse)	0.00019146	6
	Metabolic pathways - Mus musculus (mouse)	0.00110251	10
	Biosynthesis of amino acids - Mus musculus (mouse)	0.00190727	4
	HIF-1 signaling pathway - Mus musculus (mouse)	0.0035315	3
	Longevity regulating pathway - multiple species - Mus musculus (mouse)	0.00441966	2
	PPAR signaling pathway - Mus musculus (mouse)	0.00806604	2
	Glycolysis / Gluconeogenesis - Mus musculus (mouse)	0.00813558	3
	Glyoxylate and dicarboxylate metabolism - Mus musculus (mouse)	0.01025453	2
	Pyruvate metabolism - Mus musculus (mouse)	0.02450717	2
	Citrate cycle (TCA cycle) - Mus musculus (mouse)	0.03940544	2
139A-120 dpi	Metabolic pathways - Mus musculus (mouse)	0.0000412	10
	Glycolysis / Gluconeogenesis - Mus musculus (mouse)	0.000172	4
	Carbon metabolism - Mus musculus (mouse)	0.000296	5
	HIF-1 signaling pathway - Mus musculus (mouse)	0.001244	3
	Cysteine and methionine metabolism - Mus musculus (mouse)	0.003018	2
	Biosynthesis of amino acids - Mus musculus (mouse)	0.006147	3
	Arginine and proline metabolism - Mus musculus (mouse)	0.00632	2
	Pyruvate metabolism - Mus musculus (mouse)	0.012394	2
	Citrate cycle (TCA cycle) - Mus musculus (mouse)	0.020208	2
	Glucagon signaling pathway - Mus musculus (mouse)	0.024713	2
139A-80 dpi	Carbon metabolism - Mus musculus (mouse)	3.8998×10^{-10}	15
	Biosynthesis of amino acids - Mus musculus (mouse)	1.9413×10^{-7}	10
	Citrate cycle (TCA cycle) - Mus musculus (mouse)	1.9661×10^{-7}	8
	Metabolic pathways - Mus musculus (mouse)	7.4289×10^{-7}	23
	2-Oxocarboxylic acid metabolism - Mus musculus (mouse)	5.5069×10^{-6}	5
	Glyoxylate and dicarboxylate metabolism - Mus musculus (mouse)	1.1987×10^{-5}	5
	Glycolysis / Gluconeogenesis - Mus musculus (mouse)	3.2015×10^{-5}	7
	Pyruvate metabolism - Mus musculus (mouse)	0.00016141	5
	Glucagon signaling pathway - Mus musculus (mouse)	0.00102569	5
	Arginine biosynthesis - Mus musculus (mouse)	0.00124941	3
ME7-180 dpi	Cysteine and methionine metabolism - Mus musculus (mouse)	0.0000172	4
	Metabolic pathways - Mus musculus (mouse)	0.0000945	15
	Carbon metabolism - Mus musculus (mouse)	0.000337	7
	Pyruvate metabolism - Mus musculus (mouse)	0.000426	4
	Citrate cycle (TCA cycle) - Mus musculus (mouse)	0.001198	4
	Glyoxylate and dicarboxylate metabolism - Mus musculus (mouse)	0.001488	3
	Oxidative phosphorylation - Mus musculus (mouse)	0.002029	5
	Parkinson's disease - Mus musculus (mouse)	0.005802	5
	Huntington's disease - Mus musculus (mouse)	0.005802	5
	Alzheimer's disease - Mus musculus (mouse)	0.008496	5

<div align="right">Continued</div>

Brain sample	Involved pathway	*P* value	Acetylated Protein in Diff Exp
ME7-120 dpi	Carbon metabolism - Mus musculus (mouse)	4.6223×10^{-15}	23
	Biosynthesis of amino acids - Mus musculus (mouse)	1.511×10^{-10}	15
	Glycolysis / Gluconeogenesis - Mus musculus (mouse)	7.3068×10^{-9}	12
	Metabolic pathways - Mus musculus (mouse)	1.5321×10^{-8}	34
	Pentose phosphate pathway - Mus musculus (mouse)	6.5226×10^{-6}	7
	Citrate cycle (TCA cycle) - Mus musculus (mouse)	8.4311×10^{-6}	8
	Arginine biosynthesis - Mus musculus (mouse)	0.00026325	4
	RNA degradation - Mus musculus (mouse)	0.00042343	5
	HIF-1 signaling pathway - Mus musculus (mouse)	0.000782	6
	Pyruvate metabolism - Mus musculus (mouse)	0.00155492	5
ME7-80 dpi	Carbon metabolism - Mus musculus (mouse)	1.1992×10^{-16}	28
	Metabolic pathways - Mus musculus (mouse)	2.9039×10^{-13}	51
	Biosynthesis of amino acids - Mus musculus (mouse)	2.0746×10^{-11}	18
	Citrate cycle (TCA cycle) - Mus musculus (mouse)	2.777×10^{-10}	13
	Glycolysis / Gluconeogenesis - Mus musculus (mouse)	3.7415×10^{-9}	14
	2-Oxocarboxylic acid metabolism - Mus musculus (mouse)	1.8879×10^{-5}	6
	Necroptosis - Mus musculus (mouse)	2.5058×10^{-5}	8
	Pentose phosphate pathway - Mus musculus (mouse)	7.7631×10^{-5}	7
	Central carbon metabolism in cancer - Mus musculus (mouse)	0.00014251	7
	Pyruvate metabolism - Mus musculus (mouse)	0.00014251	7

Supplementary Table S3. The folds of the differentially expressed proteins within the pathway of citrate cycle (TCA cycle) in the brain samples of 139A- and ME7-infected mice collected at mid-early (80 dpi), mid-late (120 dpi) and terminal (180 dpi) stages

Diff Exp Proteins	Modification	ME7-80 dpi	139A-80 dpi	ME7-120 dpi	139A-120 dpi	ME7-180 dpi	139A-180 dpi
In 180 dpi							
Fumarate hydratase	N-Term (TMT6plex); K5 (Acetyl); Q10 (Deamidated)	1.032	1.326	2.307	1.298	1.17	1.546
Malate dehydrogenase	N-Term (Acetyl); N-Term (TMT6plex); Q2 (Deamidated); K11 (TMT6plex)	0.919	1.139	2.411	1.498	1.507	2.075
Fumarate hydratase	N-Term (TMT6plex); K7 (Acetyl)	0.925	1.039	1.252	1.106	1.702	1.278
Succinate dehydrogenase [ubiquinone] flavoprotein subunit	N-Term (TMT6plex); K8 (Acetyl); K15 (TMT6plex)	0.701	0.832	1.919	1.102	1.775	1.12
In 120 dpi							
Dihydrolipoyllysine-residue succinyltransferase component of 2-oxoglutarate dehydrogenase complex	N-Term (TMT6plex); K2 (TMT6plex); K7 (TMT6plex); K8 (Acetyl)	0.57	0.542	1.978	1.926	0.776	1.161
Pyruvate dehydrogenase E1 component subunit alpha	N-Term (TMT6plex); K2 (TMT6plex); K10 (Acetyl)	0.699	0.659	2.044	1.981	0.8505	1.2335
Fumarate hydratase	N-Term (TMT6plex); K5 (Acetyl); Q10 (Deamidated)	1.032	1.326	2.307	1.298	1.17	1.546
Malate dehydrogenase	N-Term (Acetyl); N-Term (TMT6plex); Q2 (Deamidated); K11 (TMT6plex)	0.919	1.139	2.411	1.498	1.507	2.075

Continued

Diff Exp Proteins	Modification	ME7-80 dpi	139A-80 dpi	ME7-120 dpi	139A-120 dpi	ME7-180 dpi	139A-180 dpi
Succinate--CoA ligase [ADP-forming] subunit beta	N-Term (TMT6plex); K10 (Acetyl); K11 (TMT6plex)	0.586	0.795	1.694	1.244	1.047	1.273
Isocitrate dehydrogenase [NAD] subunit alpha	N-Term (TMT6plex); K8 (Acetyl); N10 (Deamidated); M12 (Oxidation)	0.8175	0.954	1.867	1.4855	1.047	1.346
Dihydrolipoyl dehydrogenase	N-Term (TMT6plex); K5 (Acetyl); M6 (Oxidation); M7 (Oxidation); K10 (TMT6plex)	0.424	0.56	1.6	0.916	0.824	0.842
Succinate dehydrogenase [ubiquinone] flavoprotein subunit	N-Term (TMT6plex); K8(Acetyl); K15 (TMT6plex)	0.701	0.832	1.919	1.102	1.775	1.12
In 80 dpi							
Dihydrolipoyl dehydrogenase	N-Term (TMT6plex); K5 (Acetyl); M6 (Oxidation); M7 (Oxidation); K10 (TMT6plex)	0.424	0.56	1.6	0.916	0.824	0.842
Citrate synthase	N-Term (TMT6plex); K4 (TMT6plex); K10 (Acetyl)	0.362	0.515	1.09	0.944	0.675	0.814
Malate dehydrogenase	N-Term (TMT6plex); N1 (Deamidated); K6 (Acetyl); K13 (TMT6plex)	0.5	0.664	0.809	0.856	0.706	1.106
Pyruvate dehydrogenase E1 component subunit alpha	N-Term (TMT6plex); K2 (TMT6plex); K10 (Acetyl)	0.699	0.659	2.044	1.981	0.8505	1.2335
Dihydrolipoyllysine-residue succinyltransferase component of 2-oxoglutarate dehydrogenase complex	N-Term (TMT6plex); K2 (TMT6plex); K7 (TMT6plex); K8 (Acetyl)	0.57	0.542	1.978	1.926	0.776	1.161
Isocitrate dehydrogenase	N-Term (TMT6plex); C5 (Carbamidomethyl); K6 (Acetyl); N7 (Deamidated)	0.484	0.607	1.088	0.846	0.804	0.812
Aconitate hydratase	N-Term (TMT6plex); K6 (Acetyl); N7 (Deamidated); N9 (Deamidated)	0.452	0.56	1.201	1.061	0.794	0.786
Isocitrate dehydrogenase [NAD] subunit alpha	N-Term (TMT6plex); K10 (Acetyl); C15 (Carbamidomethyl); K20 (TMT6plex)	0.627	0.583	0.707	0.917	0.838	0.674
Pyruvate dehydrogenase E1 component subunit beta	N-Term (TMT6plex); K7 (Acetyl); K8 (TMT6plex)	0.643	0.701	0.996	0.88	0.8255	1.0335
Succinate--CoA ligase [ADP-forming] subunit beta	N-Term (TMT6plex); K10 (Acetyl); K11 (TMT6plex)	0.586	0.795	1.694	1.244	1.047	1.273
Isocitrate dehydrogenase [NADP]	N-Term (TMT6plex); K8 (Acetyl)	0.597	0.7445	1.261	1.1625	0.9805	1.023
Fumarate hydratase	N-Term (TMT6plex); M3 (Oxidation); K6 (Acetyl)	0.5255	0.707	1.3715	1.027	0.7775	1.176
Succinate dehydrogenase [ubiquinone] flavoprotein subunit	N-Term (TMT6plex); N-Term (Acetyl)	0.578	0.818	1.204	1.01	0.706	1.006
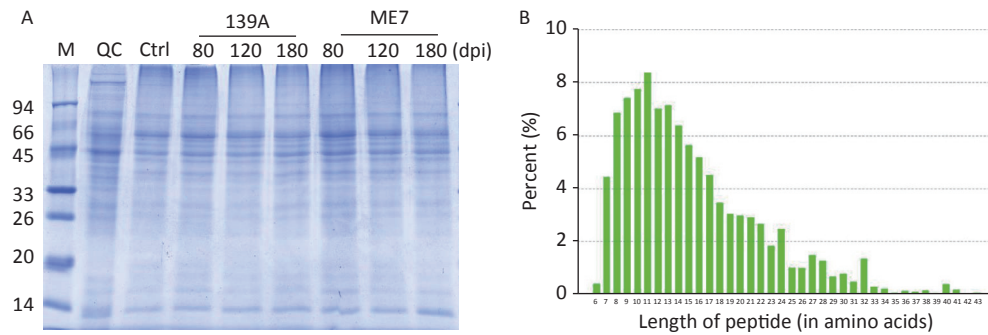
Supplementary Figure S1. Quality control and determination of the prepared samples for proteomic assays. (A) Analysis of the proteins in each sample with 12% SDS-PAGE with Coomassie blue staining. (B) Distribution of digested peptides in the length of an amino acid after searching the Swiss-Prot database. The peptides length in an amino acid is shown on the X-axis and the frequency of peptides on the Y-axis.
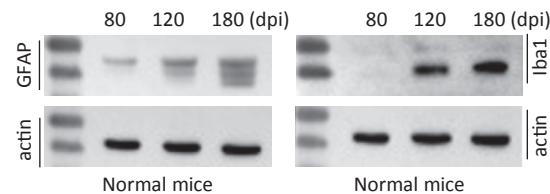
Supplementary Figure S2. Western blot evaluations of GFAP and Iba1 in the brain tissues of normal mice collected at mid-early, mid-late, and terminal stages corresponding to the infected mice. The brain homogenates from three individual infected mice collected at different time points were pooled and used as representative samples.